Journal Homepage: http://ijcpe.uobaghdad.edu.iq
Iraqi Journal of Chemical and Petroleum Engineering
Vol. 25 No. 4 (December 2024) 1 – 14
EISSN: 2618-0707, PISSN: 1997-4884

Modeling of asphaltene precipitation - part I: comparative study for asphaltene precipitation envelope prediction methods

Ali A. Ali [a, b, *], Ghassan H. Abdul-Majeed [c], Abdalellah O. Mohmmed [d]

a Department of Petroleum Engineering, College of Engineering, University of Baghdad, Baghdad, Iraq
b Department of Oil and Gas Engineering, University of Technology, Baghdad, Iraq
c College of Engineering, University of Baghdad, Baghdad, Iraq
d Department of Mechanical and Sustainable Energy, De Montfort University, Dubai, UAE

Abstract

The solubility of asphaltenes in crude oils is predominantly influenced by variations in temperature, pressure, and oil composition. These alterations can precipitate asphaltene deposition, resulting in diminished permeability, obstruction of wells and auxiliary surface facilities, and ultimately, a reduction or cessation of production. Therefore, it is imperative for upstream and downstream processing engineers to comprehend and predict asphaltene phase behavior to implement effective preventative and remedial strategies and minimize costs. Asphaltene precipitation can be predicted through the application of solubility and colloidal theories. In this study, cubic equations of state and cubic-plus-association equations of state are utilized as solubility theory-based methodologies. The advanced versions of the Peng-Robinson (APR78) and Soave-Redlich-Kwong (ASRK) cubic equations of state are compared with cubic-plus-association (CPA) equations of state using Multiflash software to predict fluid and asphaltene phase behavior. The simulation results demonstrate a strong correlation between the ASRK model and the CPA model, with a minor deviation from the results of the APR78 model. This observation suggests that these models can effectively predict asphaltene behavior and yield acceptable results when compared to experimental data for fluid and asphaltene. Considering the likelihood of asphaltene deposition within wells, hence, it is recommended to develop a model to determine the locations and quantities of deposition.

Keywords: Flow assurance; Asphaltene precipitation; Asphaltene onset pressure; Equation of state.

Received on 13/05/2024, Received in Revised Form on 13/07/2024, Accepted on 13/07/2024, Published on 30/12/2024

https://doi.org/10.31699/IJCPE.2024.4.1

1- Introduction

In 1826, the French scientist Niepce became the first to photograph asphaltene and assign it a scientific use. However, Boussingault, a Frenchman, subsequently came up with the name "asphaltene" in 1837 when characterizing the components of some bitumen and distillation waste and seeing its similarity to the original asphalt. Due to its intricacy, knowledge about asphaltene is quite restricted. On the other side, asphaltenes are usually linked to issues like flocculation, aggregation, precipitation, well bore blockage, and catalyst deactivation [1]. Whether it comes from coal or petroleum, asphaltene is theoretically characterized in current terms, as the typical component that is soluble in benzene or toluene but insoluble in n-pentane or n-heptane [2, 3]. Asphaltenes disperse or suspend in the crude oil in a reservoir fluid. However, adjustments to the oil's composition, pressure, or temperature can affect this equilibrium and cause precipitation problems [4]. Due to the risk of formation, wellbore, and production facility clogging, asphaltene precipitation from reservoir fluids during oil production is a severe issue [5]. The predominant theoretical methodologies for modeling asphaltene precipitation can be broadly categorized into two types, as elucidated by Li and Firoozabadi [6]: lyophilic and lyophobic models. In the lyophilic model, asphaltenes are considered soluble in oil, forming a true solution. In this context, asphaltene phase behavior in crude oils is influenced by molecular size and dispersion forces, and precipitation occurs when the solvent power of the hydrocarbon fluid decreases, resulting in classic liquid-liquid or solid-liquid phase equilibrium. Conversely, the lyophobic model posits that asphaltenes are insoluble in crude oil and are stabilized by resins that are peptized on their surface. Precipitation occurs when resins desorb from asphaltene particles, typically due to the addition of a low-molecular-weight alkane.

All other subdivisions of these models are shown in Fig. 1. The lyophilic models are based on the solubility approach and subdivided into: regular solution theory, Flory-Huggins theory, Scott-Magat theory, and equation of state (Eos) models. The lyophobic models are based on a colloidal approach and subdivided into the thermodynamic colloidal model, the thermodynamic micellization model, and the thermodynamic reverse micelle model. On the other hand, equation of state (EOS)

*Corresponding Author: Email: ali.ali2108p@coeng.uobaghdad.edu.iq

models are subdivided into: cubic equation of state, statistical association fluid theory, and cubic-plus-Association equation of state. Models utilizing the cubic EoS technique include solid models. While the oil and gas phases are modeled using cubic EoS, precipitated asphaltenes are represented in solid models as a pure dense phase (solid phase). For more details on these subdivision models, refer to Subramanian et. al [7].

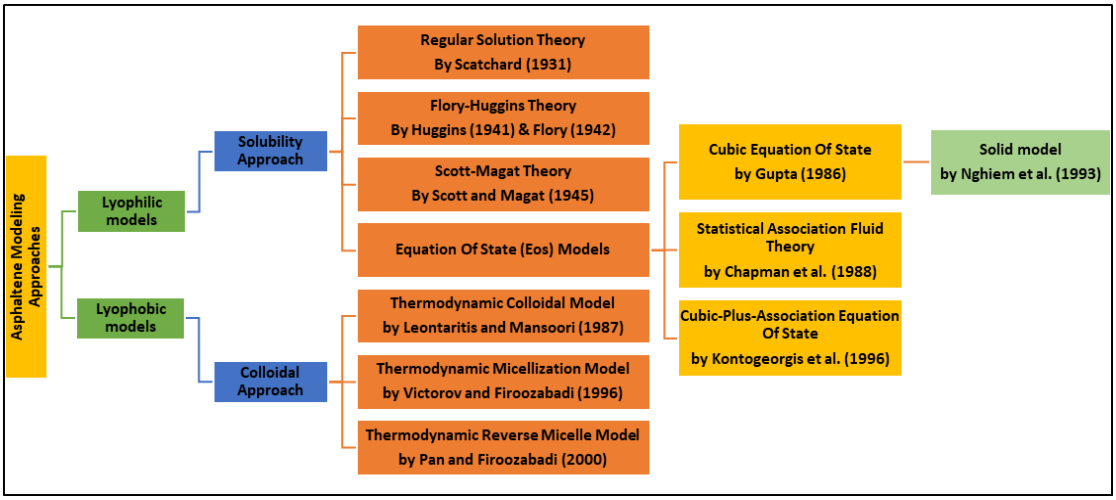

Fig. 1. Asphaltene precipitation models

The pressure at which colloidally dispersed asphaltenes precipitate at a specific temperature is known as the Asphaltene Precipitation Envelope (APE) [3]. In recent years, the cubic equation of states used widely to predict APE in addition to the phase envelope of the fluid [3, 8-13]. The cubic-plus-association equation of state (CPA EOS) gave an acceptable prediction of the asphaltene precipitation problem when compared to the statistical association fluid model and the cubic equation of state [14-16]. The asphaltene problem in oil industry of Iraq was studied by some of Iraqi researchers [17-21].

In this study, the advanced versions of Peng-Robinson (APR78) and Soave-Redlich-Kwong (ASRK) cubic equations of state are compared with cubic-plus-association equations of state (CPA EOS) in predicting the fluid and asphaltene phase behavior of an Iraqi oil field. The contribution of this investigation is to demonstrate the effect of incorporating the association term into the conventional cubic equation of state in detecting the asphaltene precipitation envelope of a live oil through the CPA EOS model and its differentiation from other conventional cubic equation of state models such as APR78 EOS and ASRK EOS. The primary conclusion of this research was that there is no discernible difference between CPA EOS with association terms and ASRK EOS in predicting the phase envelopes of the fluid and asphaltene.

2- Equation of state (Eos) models used in the present study

In this study, two types of equations of state were employed to characterize the fluid and predict the asphaltene precipitation envelope by correlating the experimental data of both the fluid and solid (asphaltene) phases.

2.1. Cubic equation of state

A cubic equation of state takes the following general form:

$$p = \frac{RT}{v-b} - \frac{a}{v^2+vb(1+c)-cb^2} \quad (1)$$

or

$$p = \frac{RT}{v-b} - \frac{a}{(v+\delta_1 b)(v+\delta_2 b)} \quad (2)$$

where:

$$2\delta_1 = (1+c) - \sqrt{(1+c)^2+4c} \quad (3)$$

$$\delta_1\delta_2 = -c \quad (4)$$

The crucial characteristics and the acentric factor are used to express the parameters a and b for pure components as follows:

$$\sqrt{a} = \sqrt{a_c\alpha} \quad (5)$$

$$\sqrt{a_c} = \sqrt{\Omega_a}(RT_c)/\sqrt{p_c} \quad (6)$$

$$\sqrt{\alpha} = 1 + k(1-\sqrt{T/T_c}) \quad (7)$$

$$b = \Omega_b RT_c/p_c \quad (8)$$

define:

$$A = ap/(RT)^2 \quad (9)$$

and

$$B = bp/RT \quad (10)$$

The compressibility factor Z ≡pv/RT can be expressed as:

$$Z^3 - Z^2(1 - cB) + Z[A - B(1 + c) - B^2(1 + 2c)] - [AB - c(B^3 + B^2)] = 0 \quad (11)$$

For mixtures, the parameters a and b are defined using the following mixing rule:

$$a = \sum_i x_i S_i \quad (12)$$

$$S_i = \sqrt{a_i} \sum_j x_j (1 - d_{ij}) \sqrt{a_j} \quad (13)$$

$$b = \sum_i x_i b_i \quad (14)$$

The advanced versions of PR EOS and SRK EOS include the ability to match stored values for liquid density through density correction of Peneloux correlation (volume-shift adjustment) and saturated vapour pressure by curve fitting, and a choice of mixing rule, either the standard Van der Waals 1-fluid mixing rule or the special Gibbs energy excess model.

a. Advanced Peng-Robinson 78 equation of state (APR78 EOS)

Eq. 1 changes to the Peng-Robinson equation of state when c=1. The parameter k in Eq. 7 is for the PR equation found from:

$$k = 0.37464 + 1.54226\omega - 0.26992\omega^2 \quad (15)$$

With the APR78 equation k is found from the same correlation if $\boldsymbol{\omega} \leq 0.49$. Otherwise the below correlation is used

$$k = 0.379642 + 1.48503\omega - 0.164423\omega^2 + 0.016666\omega^3 \quad (16)$$

b. Advanced Soave-Redlich-Kwong equation of state (ASRK EOS)

Eq. 1 changes to the Soave-Redlich-Kwong equation of state when c=0. The parameter k in Eq. 7 is for the ASRK equation found from:

$$k = 0.48508 + 1.55171\omega - 0.15613\omega^2 \quad (18)$$

Knowing Ωa, Ωb and k is required to solve the previous equations. The critical condition yields the two parameters, Ωa and Ωb. The compressibility factor will have three real, equal roots at the critical point.

$$(Z - Z_c)^3 = 0 \quad (19)$$

Comparing with the above Z equation results in:

$$\Omega_b = \frac{1}{3Z_1 + c} \quad (20)$$

$$\Omega_b = \left(Z_1^3 + c + \frac{c}{\Omega_b}\right)\Omega_b^2 \quad (21)$$

$$Z_c = \Omega_b Z_1 \quad (22)$$

Where:

$$Z_1 = 1 + Z_2 + \frac{2}{Z_2} \quad (23)$$

$$Z_2 = (3 + c + Z_3)^{1/3} \quad (24)$$

$$Z_3 = c^2 + 6c + 1 \quad (25)$$

Setting the value of c results in the usual equation of state as shown in Table 1:

Table 1. APR78 and ASRK EOS parameters

Equation of State	c	δ1	δ2	Ωa	Ωb	Zc
APR78	1	-0.4142	2.4142	0.45724	0.07780	0.307
ASRK	0	0	1	0.42747	0.08664	0.333

2.2. Cubic-plus-association equation of state (CPA EOS)

This thermodynamic model uses additional association terms to describe the self-association of asphaltene molecules and the cross-association of asphaltene and resin molecules. It is based on the well-known Soave-Redlich-Kwong (SRK) equation of state. By adding the association part to Eq. 1 and substituting c = 0, it becomes

$$p = \frac{RT}{v-b} - \frac{a}{v(v+b)} - \frac{1}{2}\frac{RT}{v}\left(1 + \rho\frac{\partial \ln g}{\partial \rho}\right)\sum_i x_i \sum_{Ai}(1 - x_{Ai}) \quad (26)$$

Eq. 26 consists of two parts: the first part represents the SRK EOS equation and is called the physical part; it is calculated in the same way as the SRK equation, and the parameters for pure compounds and mixing rules are the same; and the second part is called the association part. The crucial part of the association term is $\mathbf{x_{Ai}}$, where $\mathbf{x_i}$ is the mole fraction of component i and represents the mole fraction of site-A in a component i molecule that is not bonded to other sites. Site A on molecule i and site B on molecule j are two examples of sites on different molecules. The strength of the connection between these two sites, A_iB_J, is determined by:

$$x_{Ai} = \frac{1}{1 + \rho \sum_j x_j \sum_{Bj} x_{Bj} \Delta^{A_iB_j}} \quad (27)$$

The parameter (association strength) $\Delta^{A_iB_j}$ can be calculated from:

$$\Delta^{A_iB_j} = g(\rho)\left[\exp\left(\frac{\epsilon^{A_iB_j}}{RT}\right) - 1\right] b_{ij}\beta^{A_iB_j} \quad (28)$$

where:

$$b_{ij} = \frac{b_i + b_j}{2} \quad (29)$$

$$g(\rho) = \frac{1}{1 - 1.9\,\eta} \quad (30)$$

$$\eta = \frac{1}{4} b\rho \quad (31)$$

The parameters $\epsilon^{A_iB_j}$ and $\beta^{A_iB_j}$ are referred to as the association energy and the association volume, respectively, in the expression for the association strength $\Delta^{A_iB_j}$. Between various associating molecules, combining

criteria for association energy and volume characteristics are required. Two options have emerged from the numerous investigations as being particularly effective in a number of cases: the so-called "CR1 rule":

$$\epsilon^{A_iB_j} = \frac{\epsilon^{A_iB_i} + \epsilon^{A_jB_j}}{2} \quad (32a)$$

$$\beta^{A_iB_j} = \sqrt{\beta^{A_iB_i}\beta^{A_iB_j}} \quad (32b)$$

Alternatively, the Elliott combining rule (ECR), which use the geometric mean, may be used as follows:

$$\Delta^{A_iB_j} = \sqrt{\Delta^{A_iB_i}\Delta^{A_jB_j}} \quad (33)$$

It can be demonstrated that the equivalent formulas for the cross-association energy and cross-association volume parameters with ECR in the equation are as follows:

$$\epsilon^{A_iB_j} = \frac{\epsilon^{A_iB_i} + \epsilon^{A_jB_j}}{2} \quad (34a)$$

$$\beta^{A_iB_j} = \sqrt{\beta^{A_iB_j}\beta^{A_iB_j}}\frac{b_ib_j}{b_{ij}} \quad (34b)$$

3- Asphaltene precipitation modeling

The methodology for constructing the asphaltene model to ensure accurate results for calculations involving asphaltene-related phenomena comprises the following steps: initially, specify the asphaltene precipitation model, followed by fluid characterization. Subsequently, calibrate the model based on the PVT (pressure-volume-temperature) experiments, and further refine the model by optimizing the parameters specific to the asphaltene model. Lastly, predict the asphaltene precipitation envelope. These procedural steps are elucidated in greater detail through the flow diagram presented in Fig. 2 and will be further expounded upon in the subsequent subsections.

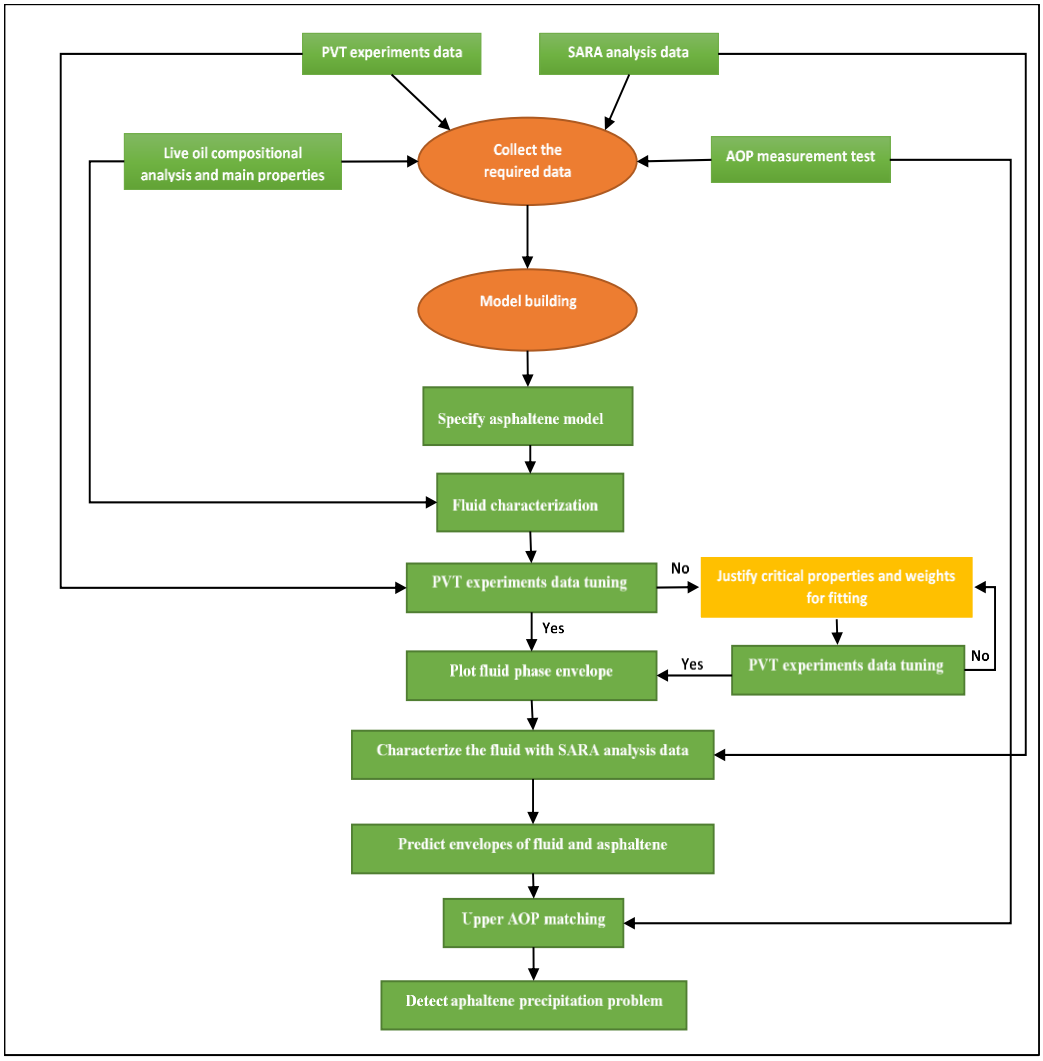

Fig. 2. The flow diagram of asphaltene precipitation modeling

3.1. Data collection

To build the precipitation model of asphaltene, the following data are required:

a. Live oil compositional analysis and main properties

The compositional analysis and the main properties of a live oil and operating conditions during production

operation have been taken from the fluid analysis report of an oil well selected for the study from one of the Iraqi oil fields, and they are shown in Table 2 and Table 3.

b. PVT experiments data

The constant composition expansion (CCE) and differential liberation (DL) tests from the reservoir fluid analysis report served as the basis for the model created by using these PVT experiments data. By doing a regression, the model can align the simulated findings with the experimental PVT data more closely.

c. SARA analysis data

An analysis technique called SARA (Saturate, Aromatic, Resin, and Asphaltene) separates these four constituents of crude oil based on their polarizability and polarity. For this study, HPLC and microasphaltene techniques were utilized to carry out SARA analysis in the fluid analysis report, and their values were taken from the report.

Table 2. Reservoir fluid composition

Component	mole%	Component	mole%	Component	mole%	Component	mole%	Component	mole%
N_2	0.467	n-C_5	2.048	C_{10}	2.309	C_{20}	0.732	C_{30}	0.297
H_2S	0.981	C_6	3.07	C_{11}	1.981	C_{21}	0.651	C_{31}	0.284
CO_2	2.678	Benzene	0.128	C_{12}	1.66	C_{22}	0.572	C_{32}	0.251
C_1	35.708	C_7	2.882	C_{13}	1.494	C_{23}	0.513	C_{33}	0.235
C_2	9.471	Toluene	0.35	C_{14}	1.338	C_{24}	0.455	C_{34}	0.218
C_3	6.089	C_8	2.627	C_{15}	1.192	C_{25}	0.414	C_{35}	0.205
i-C_4	1.035	Ethylbenzene	0.115	C_{16}	1.055	C_{26}	0.387	C_{36}^+	4.922
n-C_4	3.504	m- and p- Xylenes	0.302	C_{17}	1.017	C_{27}	0.36		
neo-Pentane	0.013	o- Xylene	0.204	C_{18}	0.898	C_{28}	0.343		
i-C_5	1.488	C_9	2.08	C_{19}	0.654	C_{29}	0.323		

Table 3. Main properties of the fluid and reservoir and operating conditions

Item	Its value	Its unit
Initial reservoir pressure	5000	psi
Current reservoir pressure	4410	psi
Reservoir temperature	111	°C
Wellhead pressure	203	psi
Wellhead temperature	23.9	°C
Gas-Oil Ratio	743	scf/bbl of residual oil at 60°F
Stocktank Oil Density	0.9059	g cm^{-3} at 0 psig and 60 °F
Bubble Point Pressure at 201°F	3135	psi

d. Measurement of asphaltene onset pressure (AOP)

Numerous methods, including the gravimetric method, light scattering method, filtration method, and acoustic resonance method, are used to evaluate AOP on live crude oil. In this study, AOP was predicted as shown in Fig. 3, which depended on the gravimetric method from the fluid analysis report.

As shown in Fig. 3, the three important properties of the fluid and asphaltene are determined, which are bubble point pressure, upper AOP, and lower AOP, at different temperatures, as follows:

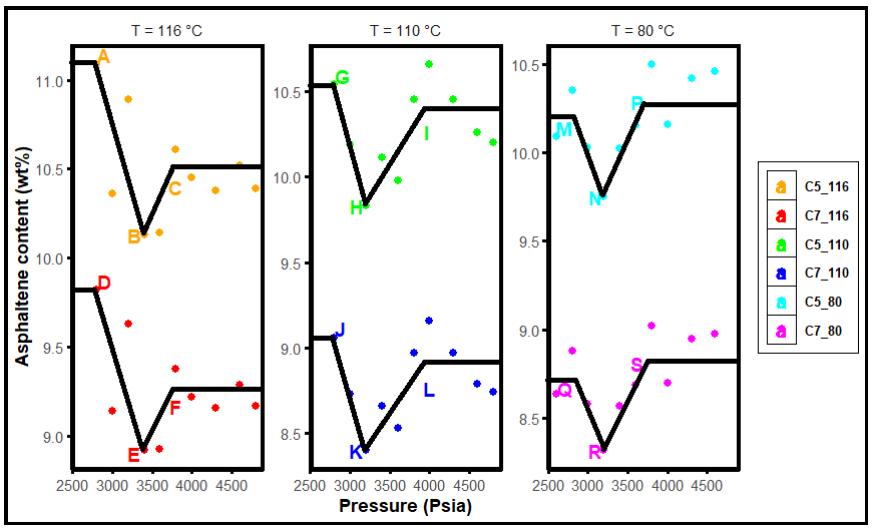

Fig. 3. AOP and pb detection at three temperature values (116, 110 and 80 ˚C)

1. By using pentane as a precipitant of asphaltene

- C, I, and P at 116, 110, and 80 ˚C, respectively, denote upper AOP points.
- B, H, and N at 116, 110, and 80 ˚C, respectively, denote bubble point pressures.
- A, G, and M at 116, 110, and 80 ˚C, respectively, denote lower AOP points.

2. By using heptane as a precipitant of asphaltene

- F, L, and S at 116, 110, and 80 ˚C, respectively, denote upper AOP points.
- E, K, and R at 116, 110, and 80 ˚C, respectively, denote bubble point pressures.
- D, J, and Q at 116, 110, and 80 ˚C, respectively, denote lower AOP points.

These properties are very useful in constructing the model of asphaltene precipitation by calibrating the simulation results with the experimental results of the properties and content of asphaltene.

3.2. Model development

Following the collection and preparation of the requisite data for model creation, as previously elucidated, encompassing information pertaining to the fluid and asphaltene, the subsequent phase involves model construction through the following procedural steps:

a. Defining asphaltene precipitation EOS

In the present study, three established models were selected to simulate asphaltene precipitation: APR78 EOS, ASRK EOS, and CPA EOS. These models have been explained theoretically and scientifically in the preceding sections.

b. Fluid characterization

Characterization is the process of creating a compositional fluid model using the data from a PVT laboratory analysis report. This stage involved using the fluid composition up to C_{36}^{+}, as shown in Table 2, to specify the system composition, after which the C_{36}^{+} fraction features like specific gravity and molecular weight were defined. The other necessary characteristics of the fluid were obtained from Table 3 to perform this step. The splitting computation was then executed in order to simulate the data and display the simulation results.

c. Tuning of the experimental PVT data

When the calculated characteristics of a fluid do not correspond to known or measured values for these fluid properties, the PVT laboratory tests (CCE and DL tests in this study) facilitated the refinement of model findings and fluid characterization by modifying model parameters and pseudo-component properties to more accurately reflect experimental data. Therefore, to validate the experimental results for the test, commence by employing the Sample QC feature. Subsequently, conduct a simulation of the experiment to evaluate how the fluid characterization and current model predict the outcomes. Lastly, refine the model to enhance its accuracy in predicting the experimental data.

At this stage, if a significant discrepancy exists in the simulation results, the critical properties of the components, including the critical pressure, critical temperature, and acentric factor, will be adjusted. The weights may also be modified for fitting purposes to align the simulation results more closely with the empirical data obtained from the experiments.

d. Plot fluid phase envelope

The phases that might be anticipated to exist under specific temperature and pressure conditions are represented by the phase envelope. In addition, it is predicted here after conducting the best calibration of the data from the PVT experiments and using the specified EOS model, as clarified in the previous steps, to represent the boundaries of the liquid and vapor phases at this stage without the presence of the asphaltene phase.

e. Characterize the fluid with SARA analysis data

From this step, until the last stage of building the model, the calibration process has been made according to the presence of asphaltenes in the fluid (oil). Through this step, the fluid was based on the SARA analysis data by identifying their proportions into the model.

f. Predict envelopes of fluid and asphaltene

In a manner similar to the previous method that was explained in the forecasting phase envelope of the fluid, the asphaltene plus fluid phase envelopes has been predicted after fluid characterization according to SARA analysis proportions.

g. AOP matching

The last and most important step in tuning the building model is regression process according to the experimental data of asphaltene onset pressure (AOP).

h. Detect asphaltene precipitation problem

Finally, the asphaltene precipitation problem can be detected through plotting the asphaltene and fluid phases envelopes. Where it contains two areas, one of which is the boundary between the liquid and gaseous phases, and the other represents the area of asphalt precipitation and is separated from the liquid and gaseous phases. What is meant by the area here are the conditions of pressure and temperature that represent the boundaries of these three phases.

4- Results and discussion

Upon completion of the asphaltene precipitation model construction, the results can be presented and discussed as follows:

4.1. Fluid characterization results

Characterizing the fluid by specifying its composition up to C_{35} and making the splitting process to the pseudo-component (C_{36}^{+}) resulted in the fluid distribution plot shown in Fig. 4. An acceptable fluid characterization result is observed in this figure when comparing the experimental amount of the mole percent of each carbon number with the simulated amount.

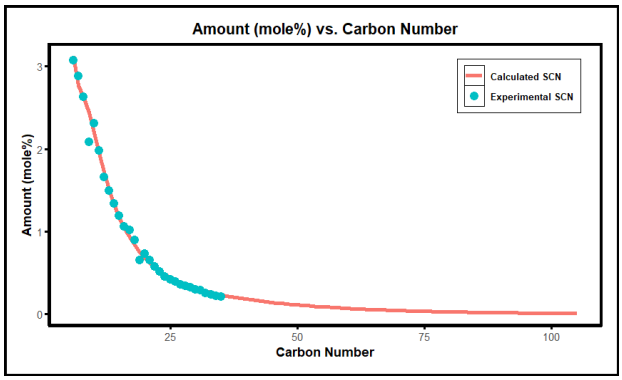

Fig. 4. Fluid distribution after splitting

4.2. Results of tuning the PVT experimental data

The results of the parameter optimization process for the three EOS models will be presented and elucidated, based on the experimental data obtained from the PVT tests. As previously noted, two categories of PVT experiments were utilized in this investigation.

a. Constant composition expansion (CCE) test data tuning

One of the most important characteristics of the fluid that is measured during this experiment is the bubble point pressure (p_b), which showed that its measured value was 3135 psi, and this number was taken from the fluid analysis report. The simulation process using the three models of cubic equation of state showed the following values of bubble point pressure:

As observed in Table 4, the three models yielded highly accurate results, closely approximating the laboratory-measured value. The CPA model demonstrated a marginal advantage due to its minimal deviation from the experimental value of the bubble point pressure.

Other CCE experimental data tuning results are shown in Fig. 5, Fig. 6, and Fig. 7. Experimentally, the relative volume (v_r) of the fluid represents the proportion of fluid volume at each pressure step that is actually present compared to that at saturation pressure (bubble point pressure in oil). The simulation outputs of this feature by EOS models showed a perfect match between the predicted data and the data of the practical experiment, noting a divergence in the points under bubble point pressure between the simulated and experimental results. The three models were also identical to each other, as shown in Fig. 5. Above bubble point pressure, there is a good match between experimental relative volume data and the simulated results, while below this pressure, the simulated values of the relative volume increased and the average deviation from actual values reached 40%. This may be caused by an error in the input data from the fluid analysis report or in the EOS calculations.

Table 4. Simulation results of bubble point pressure by three EOS models

EOS model	Simulated value of bubble point pressure, psi	| Deviation % |
CPA	3133	0.06
APR78	3131	0.13
ASRK	3132	0.1

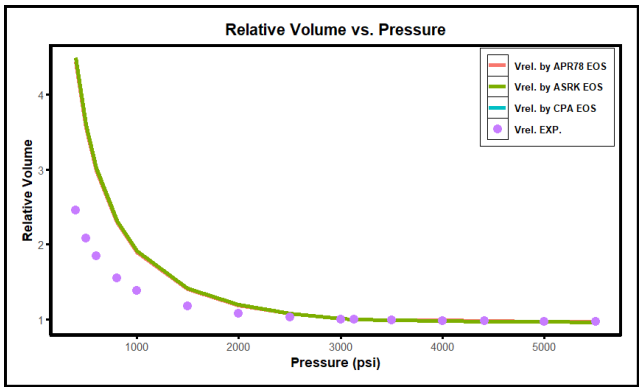

Fig. 5. Relative volume matching

The fluid density (ρ_{fluid}) versus pressure relationship above the bubble point pressure is shown in Fig. 6. As the pressure decreases from 5500 psi until it reaches the bubble point pressure, there is a decrease in fluid density due to the separation and release of gas within the fluid. In simulating this property, it was observed that the APR78 EOS model provided the best correlation between simulated and experimental results (with a maximum deviation from experimental data of 0.19%). The ASRK EOS and CPA EOS models yielded identical simulation results, exhibiting a slight divergence from the experimental data (with a maximum deviation from the experimental data of 0.34%).

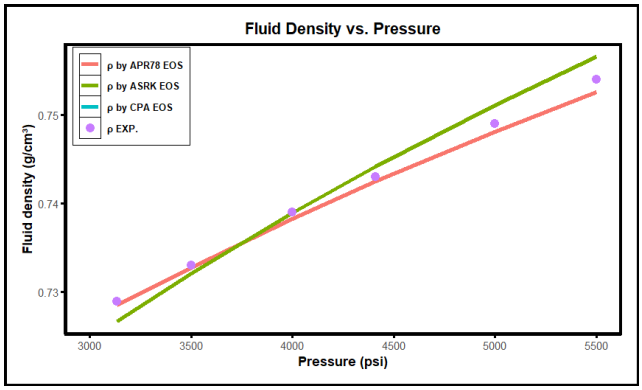

Fig. 6. Fluid density matching

Fig. 7 illustrates the simulation results of fluid compressibility (C_{fluid}) above bubble point pressure. The observed behavior differs from that of density with pressure. The compressibility of the fluid increases as pressure decreases, which can be attributed to the separation of gas bubbles above the bubble point pressure and their tendency to liberate from the oil, resulting in increased compressibility. This phenomenon aligns with the explanation provided in the previous section. The APR78 EOS model demonstrated the most accurate results, with a maximum deviation of 5%, while the other two EOS models exhibited similar performance, yielding a maximum deviation of 20%.

b. Differential liberation (DL) test data tuning

The important properties of oil and gas are calculated or determined versus pressure, down to pressures much lower than the bubble point pressure, in an experiment called the differential liberation (DL) test. These characteristics are tuned for oil and gas as follows:
1- Oil Properties: These properties are determined for different pressure points so that they are higher than the bubble point pressure and down to very low pressures, sometimes reaching atmospheric pressure. These properties are the oil density, the oil formation volume factor, and the solution gas-oil ratio (solution GOR or R_s).

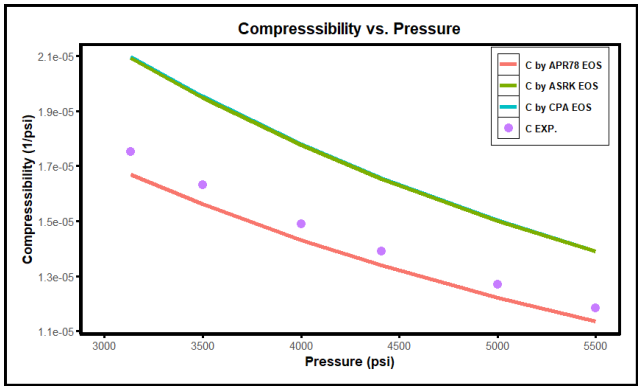

Fig. 7. Fluid compressibility matching

Fig. 8 depicts the liquid density (ρ_liquid) versus pressure relationship. Above the bubble point pressure, this relationship corresponds to that observed in the constant composition expansion (CCE) test, which represents the fluid density. Below the bubble point pressure, it represents the differential liberation (DL) test. In the region below the bubble point pressure, the APR78 equation of state (EOS) yielded a maximum deviation of 1% from the experimental value of oil density, while the CPA EOS and ASRK EOS demonstrated a maximum deviation of 0.7%.

The solution GOR (R_s) versus pressure below bubble point pressure is shown in Fig. 9. This relationship represents the volume of gas that is soluble in the oil during the depressurization process of the DL test, and its decrease is illustrated in the figure with decreasing pressure below the bubble point pressure, while it maintains a constant value for all pressures above the bubble point pressure. This phenomenon is attributed to the liberation and release of gas, which causes the volume of the solution gas to continuously decrease with pressure until it reaches zero at atmospheric pressure. This phenomenon results in the liberation of all gas dissolved in the oil, whereas above the bubble point pressure, the value remains constant due to the absence of gas release. In comparing the results of the three models for this critical characteristic of oil, the CPA EOS and ASRK EOS models demonstrated superior performance to the APR78 EOS model in predicting solution GOR, yielding deviation percentages of less than 14%, while the latter model produced a 15% deviation.

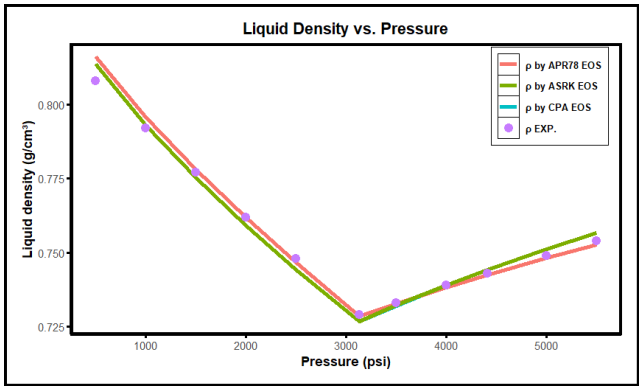

Fig. 8. Liquid density matching

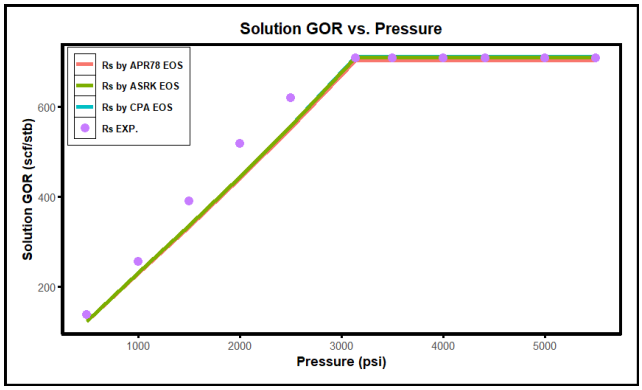

Fig. 9. Solution GOR matching

Another significant oil property is the oil formation volume factor (B_o), which represents the ratio of the volume of oil (including dissolved gas) at current reservoir pressure and temperature to the volume of oil under standard conditions. It is evident that the oil formation volume factor is always greater than or equal to unity. The simulation results for this property are illustrated in Fig. 10. CPA EOS and ASRK EOS demonstrated the highest accuracy for pressures below bubble point pressure (maximum deviation percentage of 0.6%), whereas for the remaining pressure points, three models exhibited equivalent accuracy in simulating the oil formation volume factor (maximum deviation percentage of 1%).

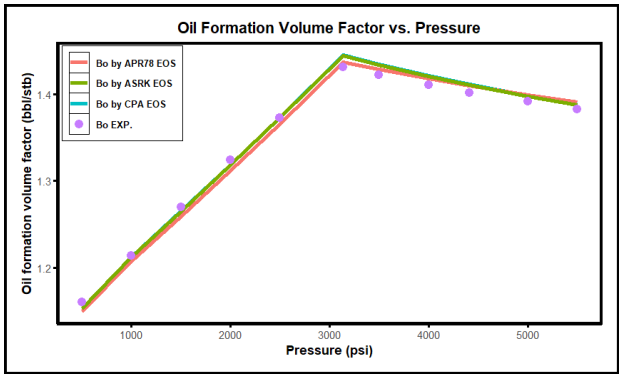

Fig. 10. Oil formation volume factor matching

2- Gas Properties: The gas properties are determined for various pressure points that are lower than the bubble point pressure and down to very low pressures, sometimes reaching atmospheric pressure. These properties are the gas gravity, the deviation factor, and the gas formation volume factor.

The gas specific gravity (SG or γ_g) simulation utilizing three models is illustrated in Fig. 11. It represents the ratio of gas density to air density under standard pressure and temperature conditions. At pressures below the saturation point, the gas released from the oil predominantly comprises lighter components. As pressure further decreases, the proportion of heavier compounds in the gas increases. This behavior is reflected in the increasing gas gravity as pressure decreases. Regarding this property, the CPA EOS and ASRK EOS models yielded identical predictions with a maximum deviation percentage of 2.6%, while the APR78 EOS model demonstrated superior agreement with a maximum deviation percentage of 1.6%.

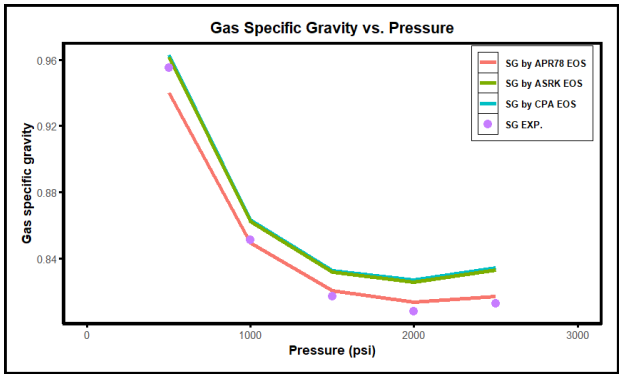

Fig. 11. Gas specific gravity matching

Fig. 12 illustrates a significant property of the gas, namely the deviation factor (Z factor). This property represents the deviation of gas behavior from ideality to reality by accounting for the limitations of ideal gas behavior assumptions, specifically considering molecular volume and intermolecular forces of attraction or repulsion. As pressure decreases, the Z factor increases due to the dominance of repulsive forces over attractive forces between molecules, resulting in an actual volume greater than the ideal volume. The maximum deviation percentage was observed with the APR78 equation of state (EOS), equaling 1.4%, while the CPA EOS and ASRK EOS yielded 0.6%.

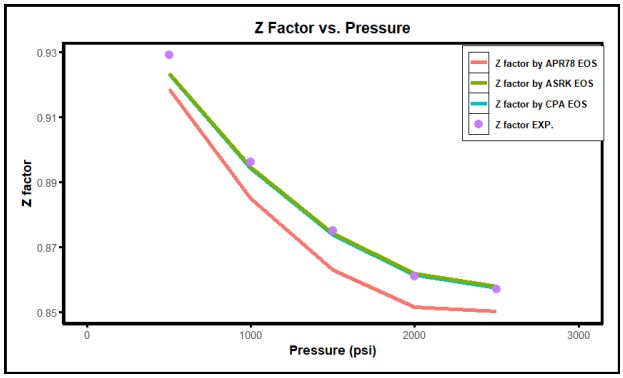

Fig. 12. Z factor matching

The final parameter in the PVT experimental data that was correlated with the experimental data in this study is the gas formation volume factor as illustrated in Fig. 13. The same trend observed in the previous gas properties is evident here, and for the same reason, an increase in (B_g) is observed as the pressure decreases. The three EOS models yielded nearly identical results and demonstrated close agreement with the experimental data for this property (maximum deviation percentage = 0.8%).

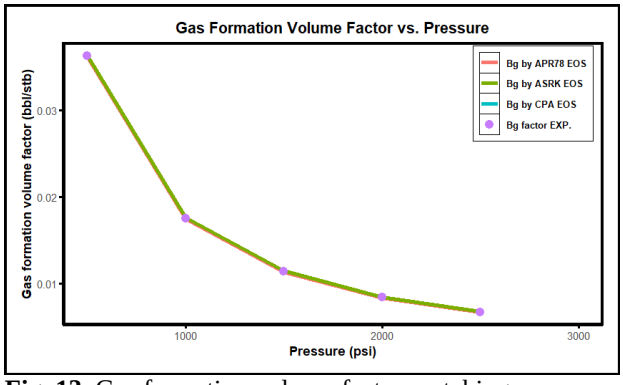

Fig. 13. Gas formation volume factor matching

Table 5 presents a summary of the comparative analysis between simulation results and experimental data, focusing on the maximum deviation from the observed measured values. The analysis employs three models: CPA EOS, ASRK EOS, and APR78 EOS.

Table 5. PVT experimental data tuning results

EOS model	CCE test data					DL test data				
	p_b	v_r	ρ_{fluid}	C_{fluid}	ρ_{liquid}	R_s	B_o	γ_g	Z_{factor}	B_g
CPA EOS	0.06%	83%	0.34%	19.7%	0.71%	14.18%	0.99%	2.61%	0.62%	0.71%
ASRK EOS	0.1%	83%	0.34%	19.5%	0.70%	14.21%	0.94%	2.45%	0.6%	0.75%
APR78 EOS	0.13%	81%	0.19%	4.8%	1.01%	14.89%	0.94%	1.55	1.37%	0.83%

4.3. Fluid phase envelope prediction

Upon completion of the process of matching the simulated results with the experimental data of PVT and obtaining satisfactory outcomes, the phase envelope (P-T diagram) for the fluid was plotted utilizing the three models, as illustrated in Fig. 14. Analysis of the figure revealed a significant convergence between the predictions of the fluid phase envelope generated by the CPA model and the ASRK model, which differed from the predictions of the APR78 model.

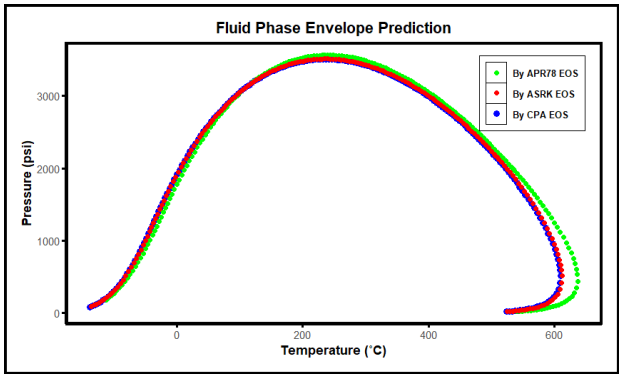

Fig. 14. P-T diagram of the fluid

4.4. Fluid and asphaltene phase envelope predictions before AOP matching

In this step, SARA analysis data for the oil was entered, and the fluid was characterized based on the proportions of the four SARA components. The three models predicted the vapor-liquid envelope (VLE) of fluid and the asphaltene precipitation envelope (APE), as shown in Fig. 15.

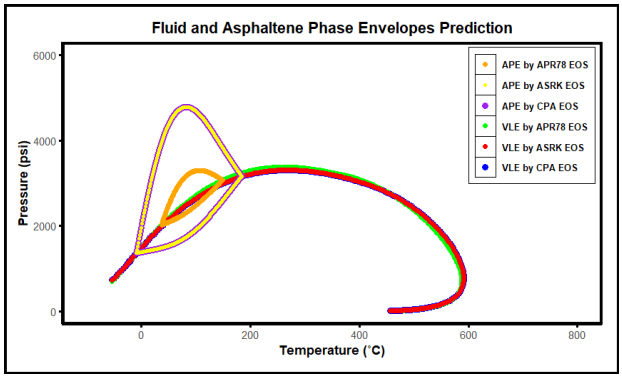

Fig. 15. P-T diagram of the fluid and asphaltene before AOP matching

Through this figure, a significant difference was observed in the prediction of the asphaltene precipitation envelope (APE) between the APR78 EOS and the two models, CPA EOS and ASRK EOS, which showed great agreement between them, as the precipitation area of the asphaltene was large with the last two models and small with the former model. While the difference was very slight when predicting the boundaries of the liquid and gaseous phases by plotting a phase diagram for the three models and the convergence between three models was greater than in the previous step when the phase boundaries were predicted.

4.5. Upper AOP matching result

The upper asphaltene onset pressure (upper AOP) curve was correlated with experimental data on this property of asphaltene, and the outcome of this calibration process by the three models of the equation of state is presented in Fig. 16. The three models yielded nearly identical results, with minimal variation between them, as illustrated in the figure. The maximum absolute error percentage was 2.2% for the APR78 EOS, while for the two other models of EOS, it was 2.1%. The three models produced logically consistent and largely acceptable results, with a notable convergence among them. The closest correlation was observed between ASRK EOS and CPA EOS, as they yielded identical matches between simulated results and experimental data for upper AOP. Fig. 16 depicts the result of the correlation process for the practical bubble point pressure, which was 3135 psi (from the fluid PVT report). An entirely analogous correlation process was generated by the three models.

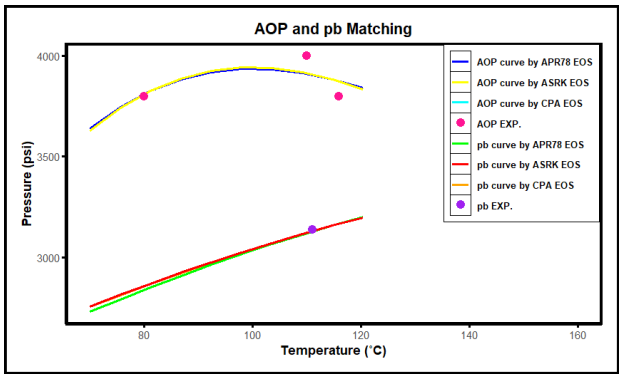

Fig. 16. Upper AOP and pb matching

4.6. Fluid and asphaltene phases envelopes predictions after AOP matching

Following the completion of all regression operations pertaining to the properties of the fluid and asphaltene, it is now feasible to predict the area of asphaltene precipitation for the selected study well by determining the pressure and temperature conditions of precipitation using these three equations of state models, as illustrated in Fig. 17. At present, the discrepancy between the three models has been reduced when predicting the phase envelopes of the fluid and asphaltene, demonstrating the significance of matching the AOP, as the variance among the three models was substantially diminished. Consequently, it is possible to rely on the results of these models in developing a strategy to prevent asphaltene precipitation. The results were closely aligned and consistent with the studies of Zhang et al. [14] and Shirani et al. [22] in predicting asphaltene precipitation conditions with AOP matching.

After projecting the initial and current pressure and temperature conditions of the reservoir onto the pressure-temperature (P-T) diagram of the fluid and asphaltene, it was determined that no asphaltene precipitation occurred under these conditions. It was observed that when the operating conditions of pressure and temperature were plotted on the diagram, the pressure decrease trajectory (pressure decline path) intersected the zone of asphaltene precipitation. This observation indicates the potential for asphaltene precipitation within the well as the pressure decreases from the bottom-hole to the wellhead. Asphaltene deposition is anticipated to occur inside the well; consequently, predictive modeling of asphaltene deposition must be conducted to determine its location and quantity.

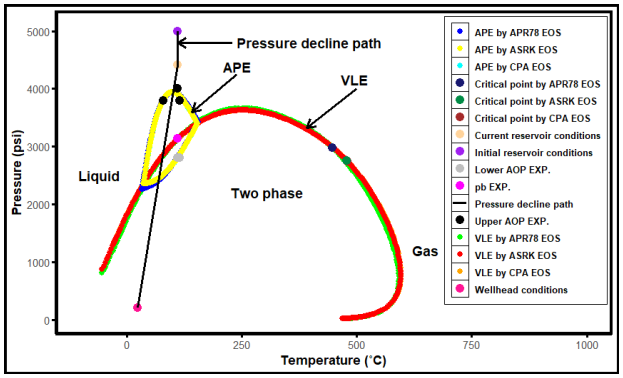

Fig. 17. P-T diagram of the fluid and asphaltene after AOP matching

5- Conclusions

The following conclusions have been drawn from the present study:

- A discrepancy was observed between the APR78 EOS model and both the ASRK EOS and CPA EOS models in simulating the data from the PVT experiments.
- The APR78 EOS and the two models, ASRK EOS and CPA EOS, exhibited disparities in their simulation and determination of the phase diagram for the fluid and asphaltene subsequent to the incorporation of SARA analysis data for oil.
- ASRK EOS and CPA EOS exhibited similar or identical performance in simulating all data from the PVT experiments and the asphaltene experiments, as well as in predicting the phase diagram of the fluid and asphaltene. This observation suggests that the association component incorporated into the CPA EOS model did not produce a substantial effect, failing to achieve a significant differentiation from the model lacking this component (ASRK EOS).
- Upon matching the experimental data of AOP, the three models yielded nearly identical simulated results and predicted the phase diagram of the fluid and asphaltene with comparable accuracy.

For future work, the deposition of asphaltene within the well is highly anticipated. Consequently, it is advisable to develop a model to determine the locations of deposition, its thickness, the extent of its impact on production, and potential methods for mitigation or prevention.

Acknowledgements

The authors express their thanks and appreciation to the Department of Oil and Gas Engineering at the University of Technology, as well as the Department of Petroleum Engineering at the University of Baghdad for their continued support and the opportunity to complete this research.

Nomenclature

Symbol	Description
a	Equation of state parameter
A	Equation of state parameter
a(T)	Energy term of equation of state
$a_{0,i}$	Parameter in the energy term for component i
$a_{0,j}$	Parameter in the energy term for component j
$a_i(T)$	The energy term of component i
$a_{ij}(T)$	Energy parameter of mixture
$a_j(T)$	The energy term of component j
AOP	Asphaltene onset pressure
AP	Asphaltene precipitation
APE	Asphaltene precipitation envelope
APR78 PR	Advanced Peng-Robinson 78
ASRK	Advanced Soave-Redlich-Kwong
b	Co-volume for pure component
b	Equation of state parameter
B	Equation of state parameter
B_g	Gas formation volume factor
B_o	Oil formation volume factor
b_{ij}	Co-volume parameter for mixture
C	Carbon
c	Equation of state parameter
$c_{1,j}$	Parameter in the energy term for component i
C_b	Average bulk particle concentration
C_{fluid}	Fluid compressibility
CCE	Constant Composition Expansion
CPA	Cubic-Plus Association
DL	Differential liberation
d_{ij}	Interaction coefficient
EOS	Equation of state
g	Radial distribution function
GOR	Gas/oil ratio
k	Equation of state parameter
p	Pressure
p_b	Bubble point pressure
R	Universal gas constant
R_s	Gas solubility
S	Equation of state parameters
SCN	Single carbon number
SG	Specific gravity
v	Volume
VLE	Vapor-liquid envelope
v_r	Relative volume
X_{Ai}	Mole fraction of site-A in molecule i not bonded to any other site/s
x_i	Mole fraction of component i

Z	Compressibility factor (pv/RT)
γ_g	Gas specific gravity
Ω_a	Equation of state parameters
Ω_b	Equation of state parameters
α	Equation of state parameter
β^{AiBj}	Association volume between site A of component i and site B of component j
Δ^{AiBj}	Association strength between site A of component i and site B of component j
δ_1	Equation of state parameter
δ_2	Equation of state parameter
η	Packing fraction
ρ	Density
ω	Acentric factor
ε^{AiBj}	Association energy between site A of component i and site B of component j

References

[1] A. A. Al Hammadi, "Modeling of asphaltene precipitation and deposition," Rice University, 2016.

[2] S. Kawanaka, K. J. Leontaritis, S. J. Park, and G. A. Mansoori, "Thermodynamic and colloidal models of asphaltene flocculation," *ACS Symposium Series*, vol. 396, pp. 443-458, 1989. https://doi.org/10.1021/bk-1989-0396.ch024

[3] A. K. M. Jamaluddin *et al.*, "Laboratory techniques to measure thermodynamic asphaltene instability," *Journal of Canadian Petroleum Technology*, vol. 41, no. 07, p. PETSOC-02-07-04., 2002. https://doi.org/10.2118/02-07-04

[4] N. E. Burke, R. E. Hobbs, and S. F. Kashou, "Measurement and modeling of asphaltene precipitation (includes associated paper 23831)," *Journal of Petroleum Technology* , vol. 42, no. 11 , pp. 1440-1446. SPE-18273-PA, 1990. https://doi.org/10.2118/18273-PA

[5] L. X. Nghiem, M. S. Hassam, R. Nutakki, and A. E. D. George, "Efficient modelling of asphaltene precipitation," in *SPE Annual Technical Conference and Exhibition, Houston, Texas, October 3-6.*, SPE-26642-MS., Oct. 1993. https://doi.org/10.2118/26642-MS

[6] Z. Li and A. Firoozabadi, "Cubic-plus-association equation of state for asphaltene precipitation in live oils," *Energy & Fuels*, vol. 24, no. 5, pp. 2956–2963, 2010. https://doi.org/10.1021/ef9014263

[7] S. Subramanian, S. Simon, and J. Sjöblom, "Asphaltene precipitation models: a review," *Journal of Dispersion Science and Technology*, vol. 37, no. 7, pp. 1027–1049, 2016. https://doi.org/10.1080/01932691.2015.1065418

[8] A. A. Ali, M. S. Al-Jawad, and A. A. Ali, "Asphaltene precipitation modeling of Sadi formation in Halfaya Iraqi oil field," *Journal of Engineering*, vol. 25, no. 8, pp. 113–128, 2019. https://doi.org/10.31026/j.eng.2019.08.08

[9] A. Ali, "Prediction of asphaltene precipitation behaviour of Khasib formation / Halfaya oil field," *Iraqi Journal of Oil and Gas Research (IJOGR)*, vol. 1, no. 1, pp. 82–95, 2021. https://doi.org/10.55699/ijogr.2021.0101.1006

[10] A. E. Shoukry, A. H. El-Banbi, and H. Sayyouh, "Enhancing asphaltene precipitation modeling by cubic-PR solid model using thermodynamic correlations and averaging techniques," *Petroleum Science*, vol. 17, no. 1, pp. 232–241, 2020. https://doi.org/10.1007/s12182-019-00377-1

[11] A. A. Ali and A. M. Aljarah, "Reservoir and fluid type determination by using equation of state / Mishrif formation / Halfaya oil field," in *AIP Conference Proceedings 2443, 030004*, 2022. https://doi.org/10.1063/5.0092324

[12] M. A. Ahmed, G. H. Abdul-Majeed, and A. K. Alhuraishawy, "Asphaltene precipitation investigation using a screening techniques for crude oil sample from the Nahr-Umr formation/Halfaya oil field," *Iraqi Journal of Chemical and Petroleum Engineering*, vol. 24, no. 1, pp. 41–50, 2023. https://doi.org/10.31699/IJCPE.2023.1.6

[13] M. A. Ahmed, G. H. Abdul-Majeed, and A. K. Alhuraishawy, "Modeling of asphaltene precipitation using CPA-EOS for live oil in an Iraqi oil well," in *AIP Conference Proceedings 2839, 020038*, 2023. https://doi.org/10.1063/5.0167684

[14] X. Zhang, N. Pedrosa, and T. Moorwood, "Modeling asphaltene phase behavior: comparison of methods for flow assurance studies," *Energy & Fuels*, vol. 26, no. 5, pp. 2611–2620, 2012. https://doi.org/10.1021/ef201383r

[15] A. Arya, X. Liang, N. von Solms, and G. M. Kontogeorgis, "Modeling of asphaltene onset precipitation conditions with cubic plus association (cpa) and perturbed chain statistical associating fluid theory (pc-saft) equations of state," *Energy & Fuels*, vol. 30, no. 8, pp. 6835–6852, 2016. https://doi.org/10.1021/acs.energyfuels.6b00674

[16] S. Alimohammadi, S. Zendehboudi, L. James, and J. Sayyad Amin, "Investigation of asphaltene precipitation; an experimental and cpa eos approaches," in *81st EAGE Conference and Exhibition 2019*, European Association of Geoscientists & Engineers, 2019, pp. 1–5. https://doi.org/10.3997/2214-4609.201901314

[17] S. A. M. Mohammed and S. D. Maan, "The effect of asphaltene on the stability of Iraqi water in crude oil emulsions," *Iraqi Journal of Chemical and Petroleum Engineering*, vol. 17, no. 2, pp. 37–45, 2016. https://doi.org/10.31699/ijcpe.2016.2.5

[18] A. A. Ali, M. S. Al-Jawad, and A. A. Ali, "Asphaltene stability of some Iraqi dead crude oils," *Journal of Engineering*, vol. 25, no. 3, pp. 53–67, 2019. https://doi.org/10.31026/j.eng.2019.03.05

[19] R. M. Hasan and A. A. Al-haleem, "Modifying an equation to predict the asphaltene deposition in the Buzurgan oil field," *Iraqi Journal of Chemical and Petroleum Engineering*, vol. 21, no. 4, pp. 49–55, 2020. https://doi.org/10.31699/IJCPE.2020.4.6

[20] L. W. Farhan, F. H. M. Almahdawi, and A. S. Hammadi, "Dissolving precipitated asphaltenes inside oil reservoirs using local solvents," *Iraqi Journal of Chemical and Petroleum Engineering*, vol. 21, no. 1, pp. 45–52, 2020. https://doi.org/10.31699/IJCPE.2020.1.7

[21] N. M. Ali and T. M. Naife, "Deasphalting of atmospheric Iraqi residue using different solvents," *Journal of Engineering*, vol. 27, no. 5, pp. 17–27, 2021. https://doi.org/10.31026/j.eng.2021.05.02

[22] B. Shirani, M. Nikazar, A. Naseri, and S. A. Mousavi-Dehghani, "Modeling of asphaltene precipitation utilizing association equation of state," *Fuel*, vol. 93, pp. 59–66, 2012. https://doi.org/10.1016/j.fuel.2011.07.007

نمذجة ترسب الإسفلتين – الجزء الأول: دراسة مقارنة لطرق التنبؤ بغلاف الترسيب الإسفلتيني

علي انور علي [١، ٢، *]، غسان حميد عبدالمجيد [٣]، عبد الإله محمد [٤]

١ قسم هندسة النفط، كلية الهندسة، جامعة بغداد، بغداد، العراق

٢ قسم هندسة النفط والغاز، الجامعة التكنولوجية، بغداد، العراق

٣ كلية الهندسة، جامعة بغداد، بغداد، العراق

٤ قسم الطاقة الميكانيكية والمستدامة، جامعة دي مونتفورت، دبي، الإمارات العربية المتحدة

الخلاصة

تتأثر قابلية ذوبان الأسفلتين في النفوط الخام عادةً بالتغيرات في درجة الحرارة والضغط وتركيب النفط. وقد يؤدي ذلك إلى ترسب وتصلب الأسفلتين، وانخفاض النفاذية، وسد الآبار والمرافق السطحية الأخرى، وفي نهاية المطاف انخفاض أو توقف الإنتاج. لذلك، من الضروري أن يكون مهندسو العمليات التحت سطحية والسطحية قادرين على فهم سلوك الطور الأسفلتيني والتنبؤ به من أجل تنفيذ الاستراتيجيات الوقائية والعلاجية المناسبة وتوفير التكلفة. يتم استخدام نظريتي الذوبان و الغروية للتنبؤ عن ترسيب الأسفلتين. معادلات الحالة المكعبة ومعادلات الحالة المكعبة زائد الارتباط هما شكلان مختلفان من المنهجيات القائمة على نظرية الذوبان قد تم استخدامهما في هذه الدراسة. تمت مقارنة الإصدارات المتقدمة من معادلات الحالة المكعبة Peng–Robinson (APR78) و Soave–Redlich–Kwong (ASRK) مع معادلات الحالة المكعبة زائد الارتباط (CPA) في التنبؤ بسلوك طور المائع والأسفلتين. كان هناك تطابق كبير إلى حد ما بين نتائج المحاكاة لنموذج ASRK ونموذج CPA، واختلاف طفيف بين النموذجين عن نتائج نموذج APR78. ومن هذا نستنتج أنه يمكن اعتماد نتائج النماذج في التنبؤ بسلوك الإسفلتين، وبالإضافة إلى ذلك فقد أعطت نتائج مقبولة عند مقارنتها بالبيانات التجريبية للمائع والإسفلتين. من المحتمل جداً أن يكون هناك ترسيب أسفلتيني داخل البئر، لذا ينصح بتطوير نموذج لتحديد مواقع وكمية الترسيب.

الكلمات الدالة: ضمان التدفق، ترسب الإسفلتين، ضغط بداية الإسفلتين، معادلة الحالة.